



Analysis of aerosol cloud interactions with a consistent signal of meteorology and other influencing parameters

Kashif Anwar^a, Khan Alam^{a,*}, Yangang Liu^b, Zhongwei Huang^c, Jianping Huang^c, Yuzhi Liu^c

^a Department of Physics, University of Peshawar, Peshawar 25120, Pakistan

^b Environmental & Climate Science Department, Brookhaven National Laboratory, USA

^c Collaborative Innovation Centre for Western Ecological Safety, College of Atmospheric Sciences, Lanzhou University, Lanzhou 730000, China

ARTICLE INFO

Keywords:

Aerosol optical depth
Cloud droplet radius
Cloud optical depth
First indirect effect
Relative humidity
Pressure vertical velocity

ABSTRACT

Quantifying the impact of aerosols on cloud micro/macro physical properties and estimating the signature of Aerosol Cloud Interactions (ACI) is one of the challenging tasks in atmospheric sciences. The Moderate Resolution Imaging Spectroradiometer and the European Centre for Medium-Range Weather Forecasts ERA-5 reanalysis data are employed to systematically study the ACI over the monsoon region in Pakistan. Based on the monsoon occurrence and rainfall intensity, the whole region is divided into three sub-regions labeled as highly intensive (R1), moderately intensive (R2) and weak (R3) monsoon region. The results indicate that the monthly mean Aerosol Optical Depth (AOD) peaks in the summer monsoon months (Jun, Jul, Aug, Sep). The well-known Twomey effect whereby the Cloud Droplet Radius (CDR) decreases with increasing AOD holds only over R3; the opposite effects (Anti-Twomey effect) are found over R1 and R2, all passing the test of statistical significance ($p < 0.05$). The multi-year AOD is found to be positively correlated with Cloud Liquid Water Path (CLWP) and Cloud Optical Depth (COD) over R1 and R2, suggesting that thicker clouds containing more water droplets are formed in polluted atmosphere. Over R3, decreases in CLWP and COD are found with increasing AOD only when AOD is less than -0.325 . The analysis of ACI over R1 and R2 during the winter months shows similar but stronger responses of CDR, CLWP and COD to the variation in AOD. The weaker responses during the summer monsoon season may attributed to the occurrence of high level cloud and unstable atmospheric condition. Further investigation of the influences of Relative Humidity and pressure vertical velocity on the CDR-AOD relationships shows that although the magnitude of the CDR-AOD correlations change with meteorological conditions, the sign of correlations remain unchanged with meteorological conditions.

1. Introduction

Global climate change is a major socio-economic issue, where atmospheric aerosols play a critical role (Papadimas et al., 2009). These small particles can directly affect climate through scattering/absorbing solar radiation (Alam et al., 2010; Gupta et al., 2013), and by modifying cloud micro- and macro- physical properties through serving as Cloud Condensation Nuclei (CCN) and Ice Nuclei (IN) (Rosenfeld, 2000; Twomey, 1974; Lohmann, 2002). The latter mechanism is termed as Aerosol Indirect Effects (AIE) or Aerosol Cloud Interactions (ACI) (Wang et al., 2015; Saponaro et al., 2017). Although potential dependence on various dynamic processes makes the magnitude as well as sign of AIE/ACI uncertain and unpredictable (Sporre et al., 2014; Jones et al., 2009; Mahowald, 2011), the continuous improvement in the retrieval

algorithms of aerosol and cloud properties allows in-depth analysis and opens new possibilities to improve understanding ACI (Benas et al., 2020).

Satellite-based studies of AIE/ACI generally seek to correlate cloud micro/macro physical properties such as Cloud Droplet Radius (CDR), Cloud Optical Depth (COD), Cloud Liquid Water Path (CLWP), Cloud Top Pressure (CTP) to aerosols loading as measured by Aerosol Optical Depth (AOD) or Aerosol Index (AI) (Saponaro et al., 2017). Inverse relationships have been found on global (Bréon et al., 2002; Myhre et al., 2007; Nakajima et al., 2001) and regional scales (Costantino and Bréon, 2010; Ou et al., 2012). Jones et al. (2009) emphasized the regionally-based study due to the relevance of ACI to the meteorological, dynamical and thermo dynamical conditions of the region, aerosol types and cloud regimes.

* Corresponding author.

E-mail address: khanalam@uop.edu.pk (K. Alam).

<https://doi.org/10.1016/j.atmosres.2022.106241>

Received 29 October 2021; Received in revised form 6 May 2022; Accepted 7 May 2022

Available online 11 May 2022

0169-8095/© 2022 Elsevier B.V. All rights reserved.

in 1999 and 2002, respectively. They are the sun synchronous orbiting satellites operating at an altitude of 705 km with the Terra overpass time 10:30 local time (LT) and Aqua overpass time 13:30 local time (LT). MODIS senses reflected solar radiance and emitted terrestrial radiance at 36 spectral bands with wavelengths ranging from 0.4–14.4 μm . Its spatial resolution is 250 m (2 spectral channels), 500 m (5 spectral bands) and 1000 m (remaining 8 to 36 bands) and temporal resolution is 1–2 days (Sharif et al., 2015). MODIS offers an unprecedented look at the atmospheric, terrestrial and oceanic phenomenology and provide useful information, providing opportunities to study the Earth's oceanic and terrestrial characteristics such as variations in landscape, ocean pollution, concentration of bound carbon etc., (Alam et al., 2014). MODIS data are also useful for collecting statistics on aerosols loading, clouds micro and macro physical properties and the correlation between aerosols and clouds properties (Alam et al., 2011). MODIS retrieved AODs at various wavelengths globally, which has been validated extensively (Remer et al., 2005; Levy et al., 2013). Over land, 2.1 μm channel is used to measure AOD from the reflectance at the top of atmosphere. MODIS distinguish fine and coarse mode particles over the ocean using spectral bands ranging from 0.47–2.1 μm (Sharif et al., 2015). In this study, AOD data are retrieved from the MODIS Terra product (MOD08_D3, Version 6.1) using combined dark target and deep blue algorithm. The estimated uncertainty in the MODIS AOD product ranges from ± 0.05 to ± 0.15 over land and from ± 0.03 to ± 0.05 AOD over the ocean (Sharif et al., 2015). The MODIS Terra products (MOD08_D3 Version 6.1) also provide daily cloud micro and macro physical properties including (CDR, COD, CLWP and CF) at three wavelengths (1.6, 2.1 and 3.7 μm) for individual cloud phases (liquid, ice and combined) separately. The MODIS cloud data have been also validated and used globally (Platnick et al., 2016). The uncertainty in the MODIS derived CDR is in the range of 1.0 μm to 3.0 μm and for COD it ranges from 10% to 21% (Rao and Dey, 2020). The AOD and cloud data used in this study is at $1^\circ \times 1^\circ$ spatial resolution.

Meteorological variables are obtained from the ECMWF ERA-5 reanalysis data. It provides the global climate data covering from 1950 to present at various pressure levels. Its temporal resolution is hourly, horizontal resolution $0.25^\circ \times 0.25^\circ$ and vertical coverage is from 1000 hPa to 1 hPa with 37 pressure levels. The reanalysis data used in this study are retrieved at 06.00 UTC (11 LT), which is close to the MODIS Terra overpass time throughout the study area.

2.3. Method

In order to reduce the uncertainty in the estimation of ACI, the data are first filtered according to the following criteria. The AOD values greater than 1.5 are excluded to reduce the impact of identifying high pollution aerosols as clouds. Thin cloudy pixels (COD < 3) are also excluded to limit the uncertainty. In addition, only low-level warm clouds with CTP > 650 hPa and CTT > 273 K are considered (Wang et al., 2015; Kant et al., 2019; Liu et al., 2020).

To study the spatiotemporal variations in aerosols and clouds, we examine the monthly climatology of aerosols (AOD) and cloud properties (CDR, COD, CLWP) by averaging significant number of daily data over the study regions. The following steps are taken to identify ACI. From the histogram of AOD, CDR, COD, CLWP data, 95% of the most frequent ranges are selected for further investigation by filtering out 2.5% extremes, providing more statistically robust data. In order to investigate the correlations between aerosols and clouds properties, the matched samples of AOD, CDR, COD and CLWP are divided into various subsets according to AOD with 0.05 AOD intervals. The intermediate value of AOD and mean value of cloud parameter (CDR, COD, CLWP) in each subset are calculated and plotted on logarithmic scales. To observe the seasonal impact on aerosol-cloud correlations, the data are sorted into winter and summer monsoon subsets. There are also some other factors that affect the actual quantitative aerosols impacts on clouds. The AOD-CDR correlation are affected by the wind direction as well as

the competition of aerosol particles for the available humidity (Liu et al., 2021). These meteorological and aerosols impacts are closely intermingled at the same time but not well understood. Thus, an effort is also made to isolate the aerosols impacts from meteorological factors such as RH and dynamic motion of air.

The aerosols First Indirect Effect (FIE) is defined as a change in CDR with respect to a change in AOD for a constant CLWP. To ensure how a change in CDR depends on a change in AOD for a constant CLWP, the following formulation is adopted from previous studies (Qiu et al., 2017; Manoj et al., 2012; Saponaro et al., 2017):

$$FIE = - \left. \frac{\partial \ln CDR}{\partial \ln AOD} \right|_{CLWP} \quad (1)$$

The FIE is calculated by dividing the CDR and AOD over different CLWP bins and then by performing a linear regression with the logarithms of AOD and CDR in each CLWP bins. Eq. (1) is equivalent to the linear model

$$\ln CDR_i = u + \alpha \ln AOD_i + \varepsilon_i \quad (2)$$

where i is the sample index, α is the exponent quantifying $\frac{\partial \ln CDR}{\partial \ln AOD}$, u is the slope of the fitting line, α and ε_i is the error term.

3. Result and discussion

3.1. Monthly climatology of aerosols and HYSPLIT backward trajectories

Fig. 2(a–c) presents the 19 years AOD climatology (obtained by averaging daily data) over R1, R2 and R3, respectively. Evidently, AOD has strong seasonality with maximums in summer monsoon and minimum in winter over all the study regions (see Fig. 2(a–c)). The strong seasonality of AOD can be well justified by the cyclic variation in meteorological conditions, and natural and anthropogenic activities over the regions. The higher values of AOD \sim greater than 1.0 in summer monsoon are due to entrance of marine aerosols such as sea salt spray and dust particles originating from Middle East, Sahara and Thar Desert (Tariq and Ali, 2015). Apart from the aerosols, the meteorological conditions (e.g., RH, temperature, pressure and wind) also play a vital role in increasing AOD during the summer season (Alam et al., 2010; Masmoudi et al., 2003). Furthermore, the high temperature during summer monsoon plays a vital role in uplifting the loose material from soil due to convection process (Alam et al., 2011). In addition, the high air temperature also holds the water vapor in air for a long time, enhancing AOD due to aerosols swelling (Masmoudi et al., 2003). Furthermore, the AODs are lower during winter season with seasonal average \pm standard deviation 0.49 ± 0.30 , 0.27 ± 0.23 , 0.56 ± 0.34 over R1, R2, R3, respectively. The lower value of AODs in winter is attributed to the wet scavenging during winter season (Alam et al., 2011). The reduced surface emission of primary aerosols from the earth surface during winter season also results in the low AOD (Zeb et al., 2019). The multi-year AODs has annual average \pm standard deviation 0.59 ± 0.20 , 0.39 ± 0.16 and 0.56 ± 0.24 over R1, R2 and R3, respectively. The high annual average AOD over R1 (0.59) and R3 (0.56) in comparison to R2 (0.39) may be attributed to the densely populated and industrial zone over R1 (Lahore, Sialkot, Faisalabad) and R3 (Karachi and Hyderabad), as compared to R2 mostly enclosed the rural areas (Kohat, Dera Ismail Khan).

The National Oceanic and Atmospheric Administration Hybrid Single Particle Lagrangian Integrated Trajectory (NOAA HYSPLIT) model is used here to analyze the origin of air masses reaching the study region. The seven-day backward trajectories at an altitude of 1500 m above the ground are shown in Fig. 3. Most of the pollutants are in planetary boundary layer varying between 1000 and 2500 m depending on seasons and regions (Zhang et al., 2020; Quan et al., 2013). Fig. 3 shows the trajectories on the typical days of summer monsoon (Fig. 3(a)) and winter season (Fig. 3(b)) that are the representative of the whole

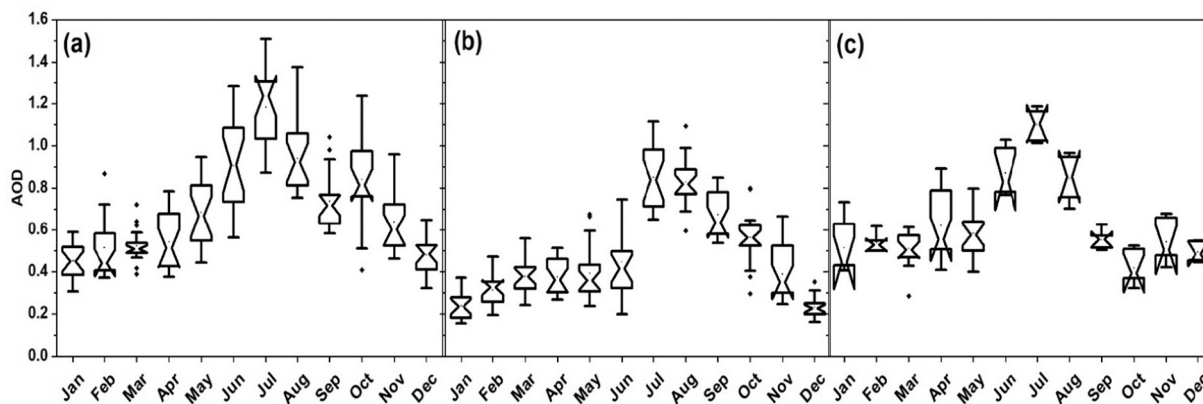


Fig. 2. Climatology of AOD at (a) R1 (b) R2 and (c) R3.

seasons. The trajectories start at 00 h UTC at particular points (shown in Fig. 3) over R1, R2, R3, respectively. Fig. 3 indicates long-range transport of air masses reaching the receptor sites during summer monsoon than winter counterpart. Therefore, it seems likely that the air masses spent more time over land during summer monsoon than winter, which would explain the higher value of AODs during summer monsoon season (Alam et al., 2011). Such long-range transport during summer monsoon also carries coarse mode aerosol particles such as sea salt and dust that also play a critical role in the elevation of AOD (Alam et al., 2011). In winter season the large portion of air masses mostly reach the study area from the nearby location. Therefore, the air masses spent less time on the continent during winter that result low value of AODs. In addition, the trajectories analyses also confirm the occurrence of offshore winds during winter season and onshore winds during summer season over R3.

3.2. Climatology of cloud properties

The 19-year climatology of cloud properties (CDR, CLWP and COD) over the study regions is shown in Fig. 4(a–i) illustrates and detailed below.

3.2.1. Climatology of CDR

The climatology of CDR (2001–2019) over R1, R2 and R3 is shown in Fig. 4a–c, respectively. The values of CDR fluctuate in the range of 9.13–20.43, 10.64–18.68 and 12.08–18.74, with the multi-year averages 14.64 ± 1.03 , 13.21 ± 0.89 and 13.39 ± 0.99 over R1, R2 and R3, respectively. The three regions exhibit almost similar seasonal variations in CDR, with peak values in the months of March/April and October/November and minimum value in Jun/July. Also, AOD varies rapidly (see Fig. 2(a–c)) during the monsoon months (Jun–Sep), while CDR varies slowly in the same months, which hint smaller AOD-CDR correlation during these months. The unstable atmospheric condition during the summer monsoon months may favor such phenomenon. Moreover, winter months exhibit slow AOD variation but strong CDR variation (Dec, Jan, Feb), which hints the stronger AOD-CDR correlation (see Fig. 4(a–c)) and (Fig. 2(a–c)). Overall, by comparing the AOD and CDR variations (Fig. 2(a–c) and Fig. 4(a–c)), both the Twomey (decrease in CDR with the increase of AOD) and Anti-Twomey are observed over the selected study regions. The Twomey effect usually occur where the increase in AOD causes increase of droplet concentration and reduction in CDR at constant CLWP. The relationship between AOD and cloud properties is detailed in Section 3.3.

3.2.2. Climatology of CLWP

Fig. 4d–f show the monthly variation in CLWP over R1, R2 and R3, respectively. The multiyear mean values of CLWP are 128.9, 111.22, 69.04 over R1, R2 and R3, respectively. CLWP also shows the seasonal variation but the seasonal amplitude is subdued, with an increasing

trend from January to May/June and decreasing trend in the remaining months. The peak value of CLWP in May/June may be due to the moist atmospheric condition with elevated water vapors during summer monsoon season. Furthermore, the AOD and CLWP variation follow almost similar increasing and decreasing trend, which hints a positive AOD-CLWP correlation. Further explanation and discussion on AOD-CLWP correlation is provided in the next sub-section.

3.2.3. Spatio-temporal variation of COD

COD also provides important information about the geometrical thickness of cloud and water contents present in cloud. Costantino and Bréon (2013) characterized the precipitating cloud as $COD > 10$ and non-precipitating cloud as $COD < 10$. Our results also reveal that the variation in COD and CLWP are interdependent because the inter-seasonal variation in COD follow almost the same pattern as CLWP discussed in previous section. The relationship between CDR, CLWP and COD follows the approximate expression $COD \sim CLWP/CDR$ as expected. As COD and CLWP are highly dependent on moisture level, which ultimately making the inter-seasonal pattern of both the quantities almost similar (Alam et al., 2014). The COD reaches its maximum value in the months of May/June due to high moisture density, and minimum value in the months of December/January due to dry atmospheric condition over R1, R2 and R3, respectively.

3.3. Relationships between AOD and cloud properties

The relationships between AOD and cloud properties (CDR, CLWP and COD) are displayed in Fig. 5(a–c). Here, the strength of aerosols impacts on clouds properties can be quantified by the slope of linear regression lines between AOD and cloud parameters on a log-log scale.

3.3.1. AOD-CDR relationships

The AOD-CDR relationships over R1, R2 and R3 are displayed in Fig. 5(a). Here AOD is used as a proxy of Cloud Condensation Nuclei (CCN). Our results reveal that AOD and CDR are positively correlated (Anti-Twomey effect), with linear regression slope of 0.09 and 0.04 over R1 and R2, respectively (see Fig. 5(a)). Various feedback mechanisms are involved in this positive AOD-CDR correlation. Yuan et al. (2008) also hypothesized that the positive correlation was due to the less soluble organic compound. In our case, the oxidation of volatile organic compound from industrial and transportation sources significantly contribute to AOD over R1 and R2. These less soluble organic compound increases the critical supersaturation (Kohler theory) for the particle to be activated, and thus less activated particles make AOD-CDR correlation positive (Yuan et al., 2008). In addition, the positive correlation may be attributed to the cloud burning effect (Wang et al., 2015; Xue et al., 2008). The primary sources of aerosols emission is vehicular, industrial, coal and crop residue burning, containing abundant absorbing

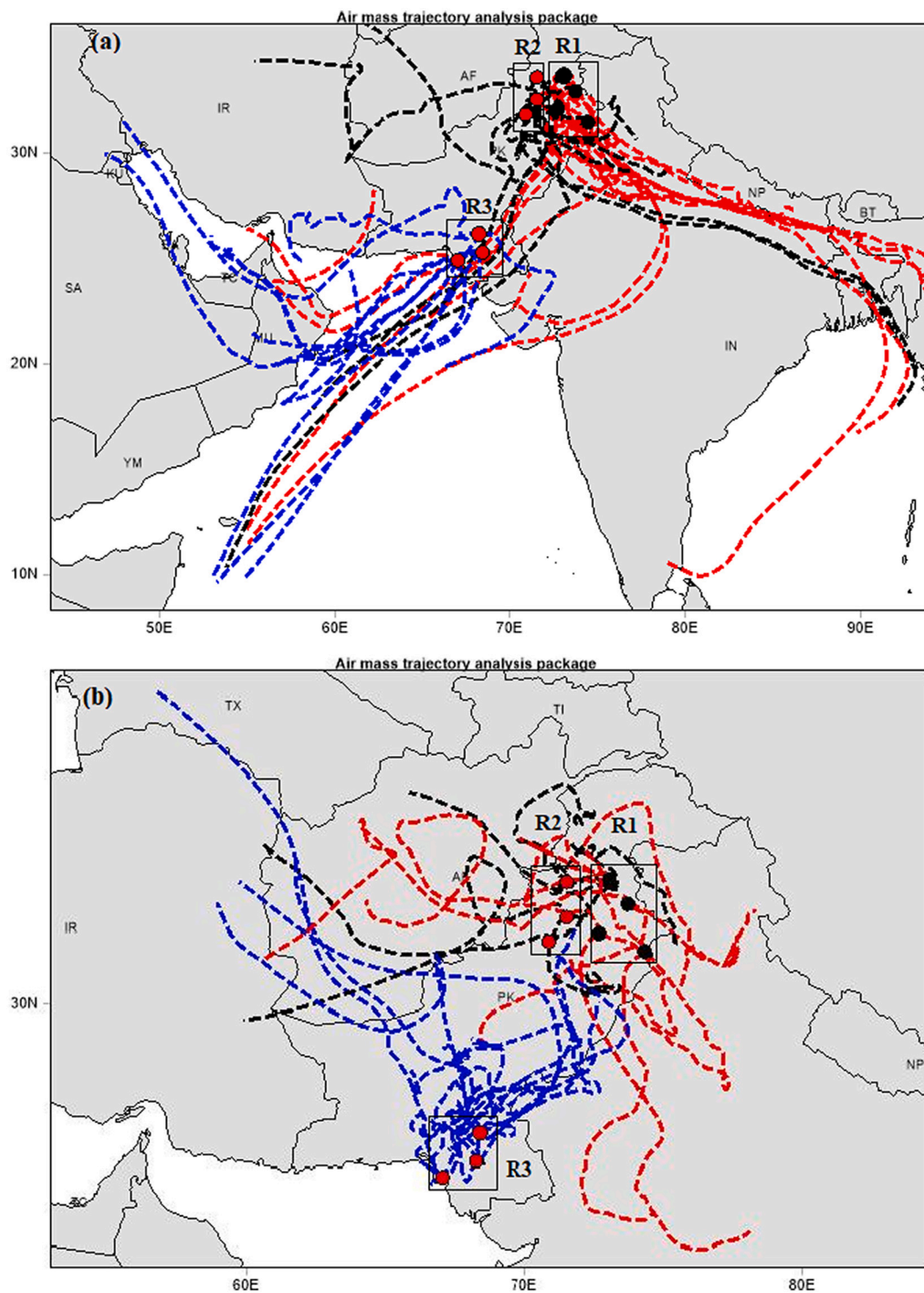


Fig. 3. Shows the HYSPLIT backward air mass trajectories at the receptor sites during (a) summer monsoon season (b) winter season. R1 trajectories are represented by red, R2 black and R3 blue color. (For interpretation of the references to color in this figure legend, the reader is referred to the web version of this article.)

aerosols such as black carbon that may trap solar radiation and evaporate smaller droplets as the number of droplets increases. Such positive correlation has also been observed over the highly industrial and urban area of Beijing-Tianjin-Hebei and Yangtze River Delta (Liu et al., 2020; Wang et al., 2014). It is also noteworthy that aerosols swelling, atmospheric dynamics and retrieval artifacts may also lead to the positive relation (Yuan et al., 2008; Jia et al., 2019). Here in our study region certain degree of influence exists for some of these factors; however, none seem to be the primary cause of the observed positive AOD-CDR

correlations (discussed in Section 3.6). It is also observed that the response of CDR to AOD is stronger over R1 than R2. Chang et al. (2017) described that the coarse-mode aerosol particles are more efficiently activated as Cloud Condensation Nuclei (CCN) than fine particles. As R1 contains a large number of coarse mode particles than R2 (Zhang et al., 2020) making the correlation stronger. Over R3 (see blue colored line in Fig. 5(a)), the AOD-CDR correlation is positive (Anti-Twomey) with slope 0.13 when $AOD < \sim 0.325$, but negative (Twomey effect) with slope -0.13 at $AOD > \sim 0.325$. This anomalous behavior over R3 may

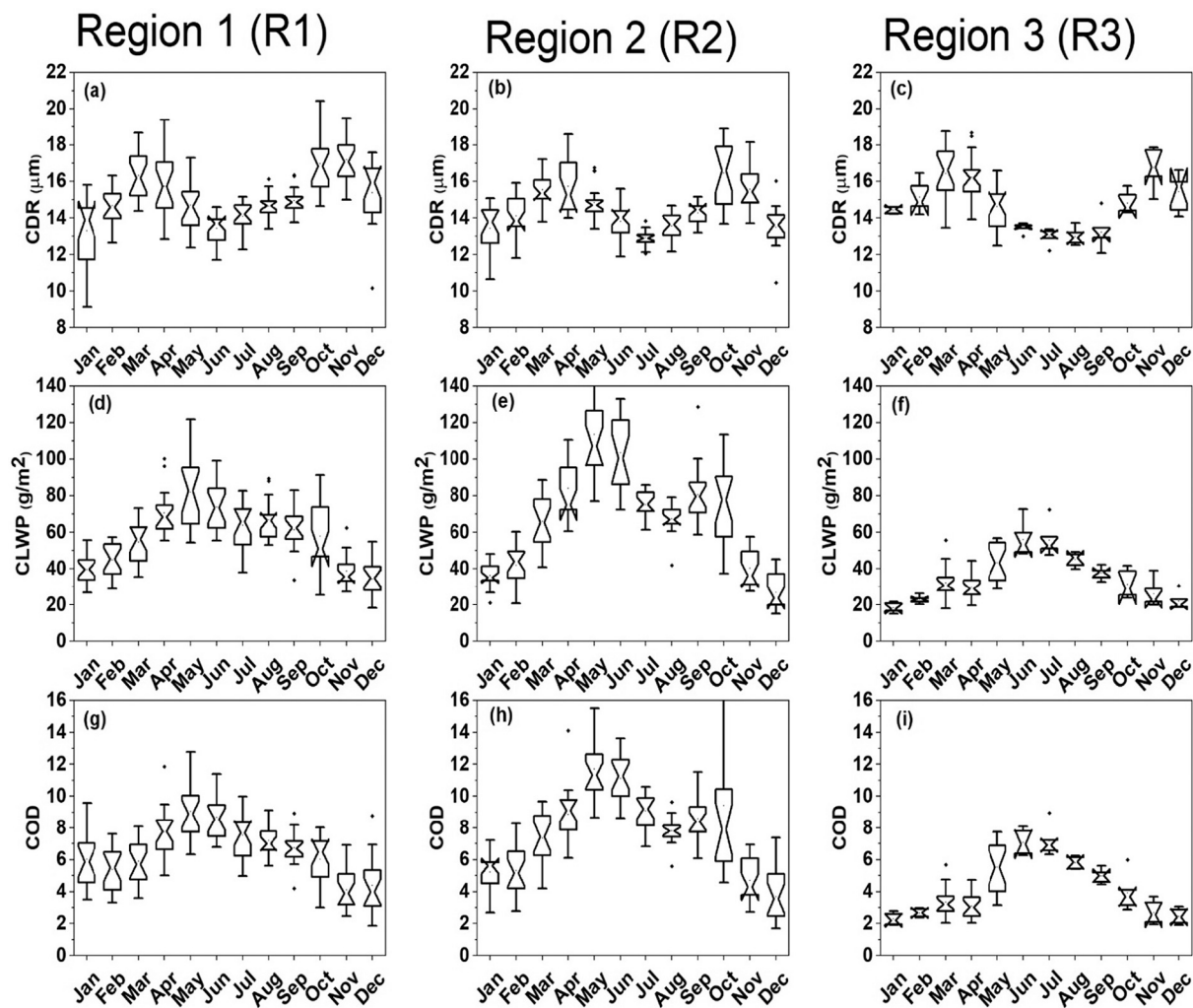


Fig. 4. Climatology of CDR, CLWP and COD over R1 (left panel), R2 (middle panel) and R3 (right panel).

be due to aerosol types, differences in the cloud properties and meteorology. Studies have observed that maritime aerosols contain sea salt (giant particles), which would not contribute much to AOD but would activate as CCN and lead to a positive AOD-CDR correlation (Lohmann and Lesins, 2003; Jones et al., 2009). On the contrary, Jones and Christopher (2008) observed the negative AOD-CDR correlation, when dust and other continental air masses comprises the large portion of total AOD. Zhao et al. (2018) also reported different regimes of AOD-CDR relationships over oceans. In our case, R3 is near to the coastal region with frequent occurrence of maritime and continental aerosols. Therefore, such response may be attributed to the differences in aerosol types such as maritime and continental aerosols. Jones et al. (2009) also emphasized that the changes in aerosol species and meteorological conditions are responsible for such behavior of AOD-CDR correlation. Also, AOD-CDR correlation is highly sensitive to CLWP (Jia et al., 2019; Liu et al., 2021). Therefore, the sharp decrease in CLWP (see blue color line in Fig. 5b) in the lower AOD ~ 0.325 and almost constant in higher AOD over R3 may also responsible for this anomalous behavior of AOD-CDR correlation.

3.3.2. AOD-CLWP correlations

Fig. 5(b) presents the AOD-CLWP correlations over R1, R2 and R3, respectively. The resulting slope of least square fitted lines are 0.33 and 0.20 over R1 and R2, respectively (see black and red colors in Fig. 5(b)). The increasing behavior of CLWP with AOD over these regions can be explained on the base of Albrecht (1989) hypothesis. They theorized

that the cloud in the polluted atmosphere contain more droplet, which consequently increase the CLWP and the cloud lifetime. Alam et al. (2014) reported that the CLWP response is also closely associated with the amount of water vapors in the atmosphere. They observed high water vapor when AOD is high over the mega cities of Pakistan. Thus, increasing trend of AOD also increase water vapor that make the slope positive over R1 and R2. Storelvmo et al. (2006) also observed that water soluble aerosol grows with the humidity swelling and this growth is a function of humidity. As aerosols grow due to water uptake, they become optically thick which leads a positive AOD-CLWP and AOD-COD correlation (Alam et al., 2014). Thus, the positive correlations observed over R1 and R2 are consistent with the findings of Storelvmo et al. (2006). The AOD-CLWP response over R3 exhibits two branches: strong negative correlation when AOD is less than ~ 0.325 and a weak positive correlation over the range of higher AOD (see blue color line in Fig. 5 (b)). Such contrasting responses over R3 may be attributed to the cloud formed under various air masses (e.g., maritime, continental), both of which are often observed in coastline regions (Han et al., 2002; Minnis et al., 1992; Twohy et al., 1995). Maritime clouds show negative sensitivity with AOD due to decoupling of cloud layers where, the continental cloud shows almost neutral/ slight sensitivity to AOD (Han et al., 2002).

3.3.3. AOD-COD correlations

The dependences of COD on AOD can be seen from Fig. 5(c). The COD-AOD relationship can be analyzed with the following equation

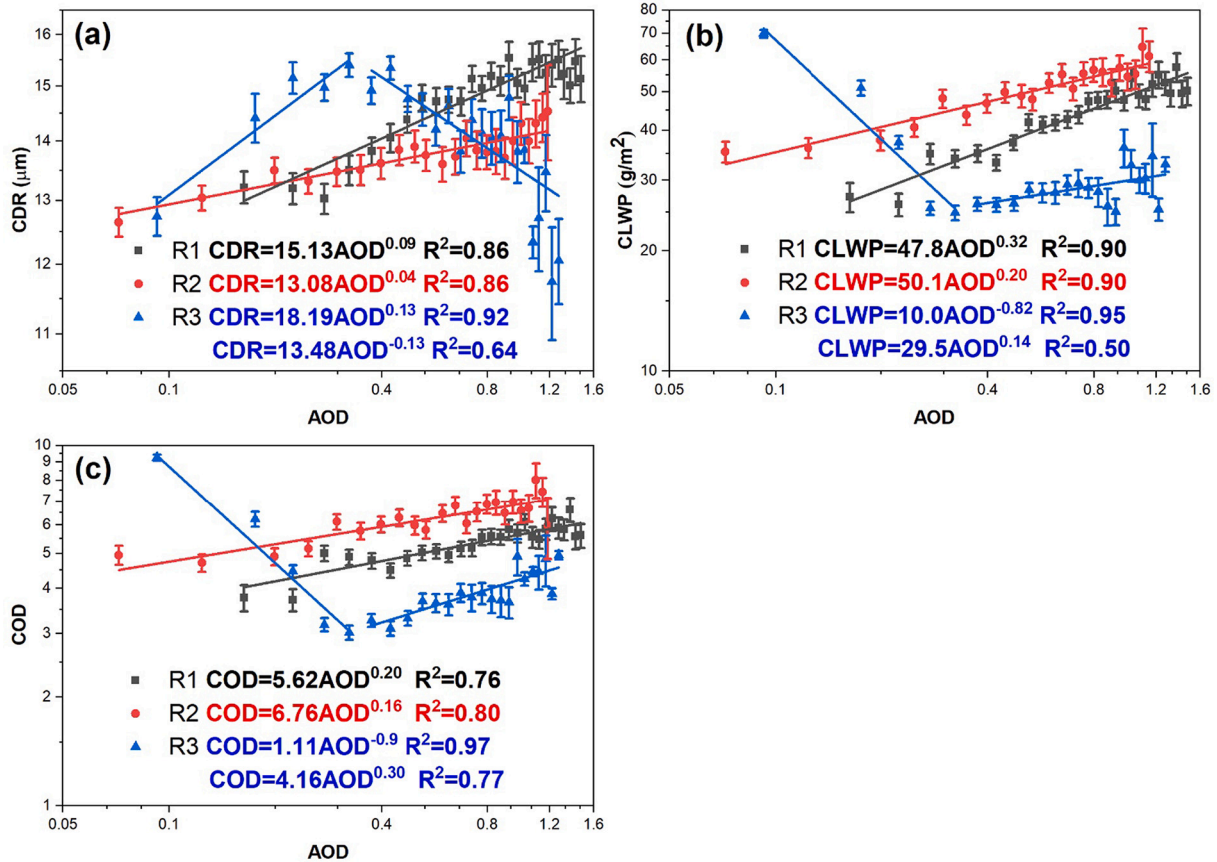


Fig. 5. (a) AOD-CDR (b) AOD-CLWP and (c) AOD-COD correlations over R1, R2 and R3. The exponent of AOD represent the slope of the fitted line in log-log scale. Error bars represents the confidence level of the mean value and is calculated by $\sigma/(n - 2)$, where σ is the standard deviation of cloud properties and n is the number of samples in AOD bin.

(Costantino and Bréon, 2013):

$$\frac{\partial \log \text{COD}}{\partial \log \text{AOD}} = \frac{\partial \log \text{CLWP}}{\partial \log \text{AOD}} - \frac{\partial \log \text{CDR}}{\partial \log \text{AOD}} \quad (3)$$

This equation shows that the response of COD to AOD can be estimated from the slope of log CLWP-log AOD and log CDR-log AOD graph. It is observed from Fig. 5(c), that the response of COD to the increase in AOD over R1, R2 and R3 are coherent with the estimated results of Eq. (3). The positive AOD-CLWP correlation makes AOD-COD correlation positive, while the negative AOD-CDR response makes AOD-COD correlation positive and vice versa.

3.4. Seasonal analysis

ACI is dependent both on aerosols properties and on vertical velocity (Feingold et al., 2001; Chen et al., 2016, 2018). Generally, the atmosphere in the summer monsoon over Pakistan is humid, unstable and more susceptible to convective cloud and frequent up drafting (Tariq and Ali, 2015). While, on the other hand winter season is dry with comparably stable atmospheric condition.

3.4.1. Seasonal comparison of AOD-CDR relationships

The aerosols effect on CDR during summer monsoon and winter subset are investigated, compared and displayed in Fig. 6(a-c). It can be seen that CDR is comparatively large during winter season over all the study regions. The lack of sufficient water vapor in atmosphere during dry winter season inhibit the growth of fine mode particle and only a subset (large) of aerosol particles active and grow with faster rate resulting larger CDR during winter season (Liu et al., 2021; Kant et al.,

2019). Thus, the larger CDR during this season indicate the existence of aerosols competition for water vapor as a dominant micro physical effect. Also, the AOD-CDR correlations is stronger during winter season (large positive slope) compared to summer monsoon (small positive slope) counterpart, over R1 and R2. Various diverse phenomenon may take part in such correlations. The unstable atmospheric condition during summer monsoon season likely makes the ACI smaller during this season. During this season meteorological component are more responsible for the observed changes in cloud micro and macro physical properties (Kant et al., 2019). Also, due to higher relative humidity during summer monsoon the hygroscopic aerosols of the same concentration may have a large extinction coefficient and higher AOD value indicating AOD may not be a good proxy for CCN and thus for analyzing ACI (Liu et al., 2021). In addition, the increase in the emission of light absorbing aerosols, caused by the burning activity during winter season increase the light absorbing aerosols which may causes the cloud burning effect (Koren et al., 2004). Wang et al. (2015) also observed a stronger AOD-CDR correlation during winter over the Eastern China. They also associated such phenomenon with the increase in the emission of light absorbing aerosols due to burning activities in winter season. Contrary to R1 and R2, such monotonic correlations are not observed over R3 during summer monsoon. The AOD-CDR correlation is positive (0.07) only when AOD is less than ~ 0.325 while, negative correlation (-0.13) are observed for the higher AOD. Such differences in the cloud micro physics occur due the formation of cloud under various air masses such as maritime and continental cloud. Region closed to the coastal line are favorable for the frequent occurrence of such phenomenon which lend credence to our results in R3. The shift of aerosol species from marine aerosols to dust aerosols and meteorological conditions that

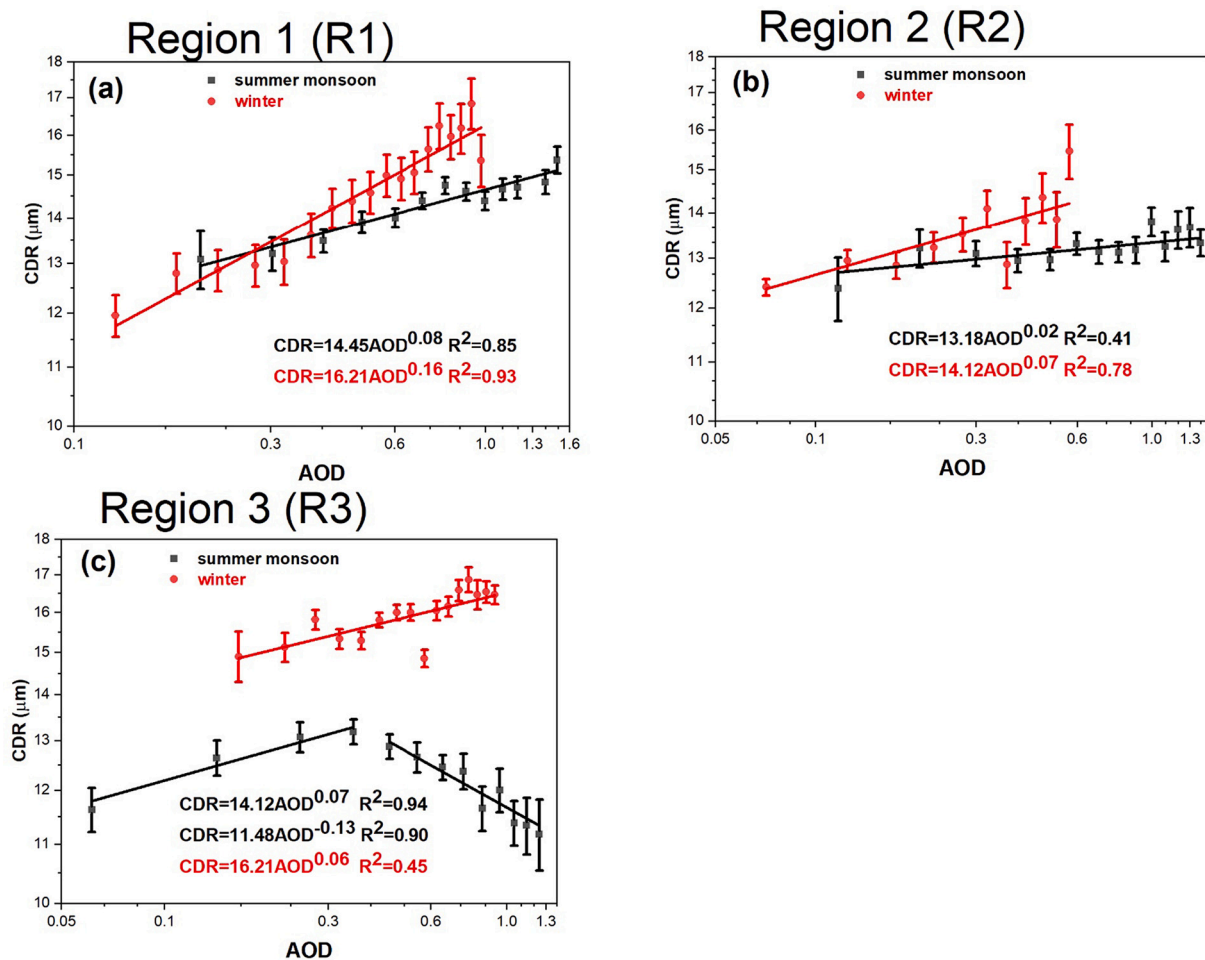


Fig. 6. Responses of CDR to the variation in AOD during monsoon and winter seasons over (a) R1 (b) R2 and (c) R3. The exponent of AODs represents the slope of the fitted line on log-log scale. Error bars represent the confidence level of the mean value of cloud parameter.

occur in summer monsoon are the also contributing to such behavior (Jones et al., 2009). The occurrence of dust and sea salt over R3 during summer monsoon (Sharif et al., 2015) making the correlation two folded during this season.

3.4.2. Seasonal comparison of AOD-CLWP correlations

The investigation of AOD-CLWP correlation plays an important role in cloud lifetime, cloud thickness and other micro and macro physical properties. Fig. 7(a–c) presents the CLWP responses to the variation in AOD in the monsoon and its winter counterpart. It can be concluded that CLWP is higher in all AOD bins during the summer monsoon season compared to the winter season. These high CLWP is due to the increase in water vapors in the atmosphere during humid summer season. It is also observed from Fig. 7 that the CLWP shows the increasing behavior with the increase in AOD (positive slopes) over R1 and R2. The comparison of the slope of the least square fitted line shown in Fig. 7(a) and (b) indicate that the sensitivity of CLWP to AOD get weaker in monsoon (small slope) compared to winter (large slope) over R1 and R2. This phenomenon is due to widespread and diverse cloud conditions and the regional heterogeneity of aerosols and clouds during summer monsoon. Our results are consistent with the finding of Pan et al. (2018), who also observed a weaker AOD-CLWP correlation in monsoon. Furthermore, Pan et al. (2018) also investigated that the ACI is gradually weakening with Cloud Based Height (CBH) because most of aerosols (75%) occur below 3 km. They also observed frequent high CBH cloud in summer monsoon season. Therefore, the low sensitivity of CLWP to AOD observed in summer monsoon can be attributed to the occurrence of

high-level clouds. It can also be inferred from Fig. 7(c), that over R3, there is a strong negative AOD-CLWP correlation only when AOD is below ~ 0.325 but a weaker sensitivity for higher AOD bins during monsoon season. Such responses are due to the frequent occurrence of marine and pollution aerosols. The strong onshore wind blowing during summer monsoon carry giant sea salt and other absorbing aerosols such as dust and other continental aerosols to R3. The marine aerosols coupled with high surface temperature results in the strong negative sensitivity to CLWP when AOD is less than ~ 0.325 . Also, from Fig. 7(c), a weak sensitivity of CLWP to all AOD bins can be observed over R3 during winter season. The weaker response over R3 during winter season may be attributed to the strong offshore wind during this season, which ultimately reduces ACI.

3.4.3. Seasonal comparison of AOD-COD relationships

Fig. 8(a–c) shows the responses of COD to the variation in AOD. COD is comparatively high during summer monsoon as compared to winter over R1, R2 and R3. Alam et al. (2014) proposed that COD is strongly dependent on moisture level since as the density of moisture increase in summer monsoon the value of COD increase and vice versa. Moreover, the sensitivities of COD to the variation in AOD are weaker in monsoon compared to winter and vice versa. The weaker responses during summer monsoon may be due to occurrence of high-level clouds that consequently weakens ACI. The impact of aerosols is more prominent in low level clouds that are likely better coupled with aerosols in the atmospheric boundary layer (Pan et al., 2018). Also, the dynamic and thermodynamic processes during summer monsoon make an unstable

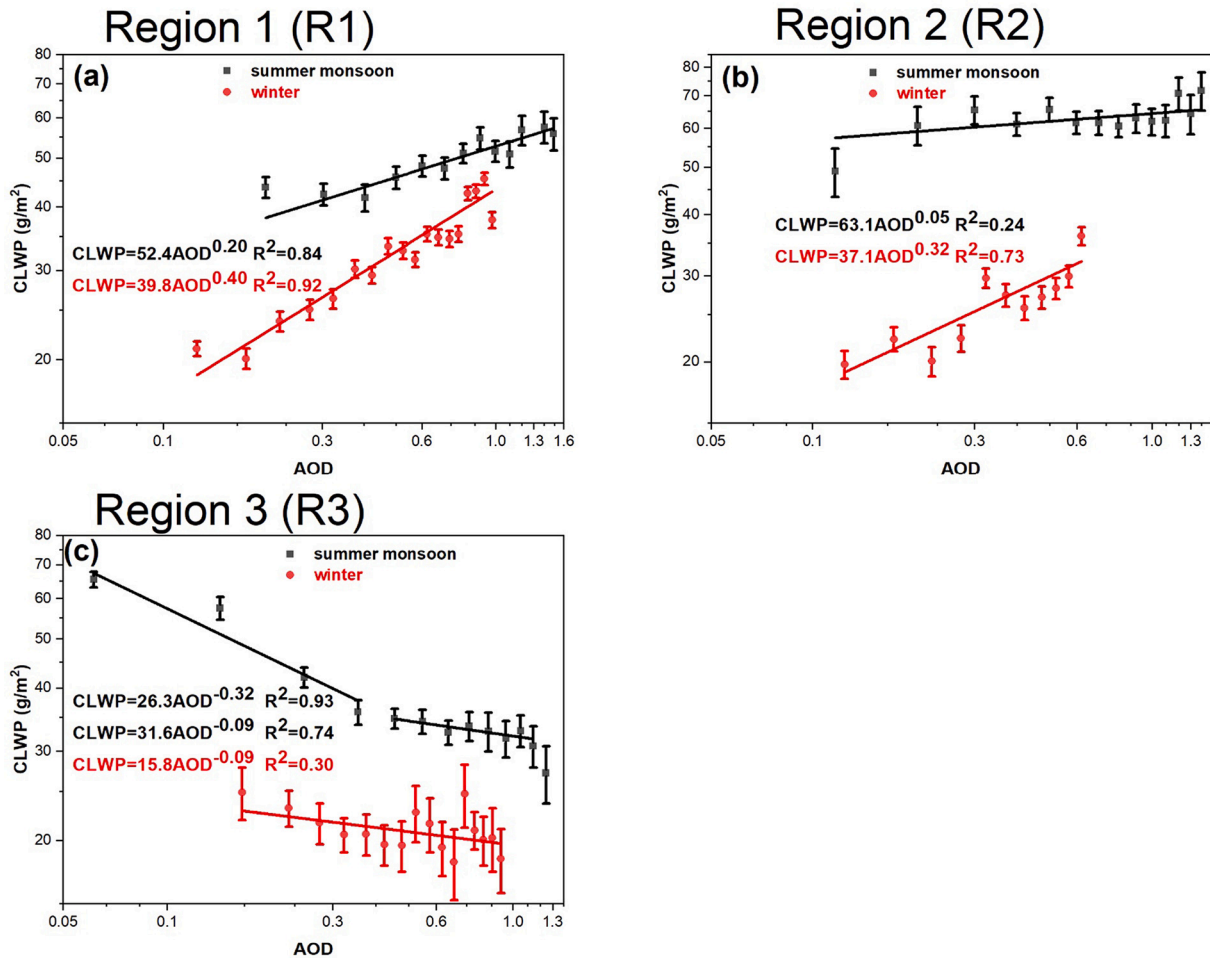


Fig. 7. Same as Fig. 6 but for the CLWP.

atmospheric condition, masking ACI (Kant et al., 2019).

3.5. Relationships between AOD and cloud macrophysical variables

3.5.1. AOD-CTP relationships

Analysis of AOD-CTP correlation is also important because CTP is a key variable for determining the sign of cloud radiative effects (from cooling to warming) (Liu et al., 2020). Irrespective of the environmental condition, the occurrence frequency of CTP in various AOD ranges are examined over R1 (see Fig. 9a), R2 (see Fig. 9b) and R3 (see Fig. 9c). The collected data are first sorted into seven equal sized subsets according to different AOD bins. Then, the frequency of occurrence of various CTP levels (650–700, 700–750, 750–800, 800–850, 850–900, 900–950 and 950–1000) are examined in each AOD bin and shown by a stacked diagram (see Fig. 9). Various features of AOD-CTP correlations can be explained from Fig. 9. The occurrence frequency of low-level clouds (CTP: 900–950 and 950–1000) decreased at higher AOD bins and vice versa (see Fig. 9(a–c)). Therefore, we conclude that the increase in AOD invigorate the high level (low CTP) clouds over all the regions. Sharif et al. (2015) interlinked the decrease in CTP at higher AOD bins to the suppression of precipitation by increasing the cloud life time thus affecting the CTP and cloud albedo. Some studies have also analyzed the role of meteorological variable such as updraft velocity and wind direction on AOD-CTP correlation (Tripathi et al., 2007; Koren et al., 2005). They suggested that updraft velocity is strongly correlated with changes in CTP.

3.6. Effect of meteorological variables on AOD-CDR relationships

3.6.1. RH effect on AOD-CDR correlations

RH is one of the key factors influencing the growth of aerosol particles and clouds formation. Previous observational studies have reported that RH at cloud base is closely associated with cloud properties, particularly low-level warm clouds (Wang et al., 2014; Small et al., 2011; Jeong et al., 2007). Therefore, it is very important to figure out the role of RH on ACI.

In order to investigate the role of RH on AOD-CDR correlations, the datasets are stratified into three equal sized subset of RH and the mean of each subset are calculated. The averages of lowest tercile of RH (36%, 33%) represent the driest condition while, the averages of highest tercile of RH (76%, 73%) represent the wettest condition over R1, R2, respectively. It can be deduced from Fig. 10, that CDR is high in the low % RH range (dry condition) compared to high % RH limit (moist condition) over all AOD bins, which is due to water vapor competition effect. When enough water vapors are not present at cloud base (dry condition), only a subset of particles are activated and grow with fast rate, making average CDR greater at low % RH. Also, the slope of the regression line under the high RH (moist condition) is over all more positive (greater slope) than those under low % RH condition (dry condition), which is indicative of more sensitivity of CDR to AOD at high % RH condition. Overall, from Fig. 10, we conclude that AOD-CDR correlations are positive under both dry and moist condition. However, the magnitude of the correlations is a function of the RH condition. In addition, R3 is not included in this sub section because in the low AOD limit ~ 0.325 the number of data samples is too low in the driest and

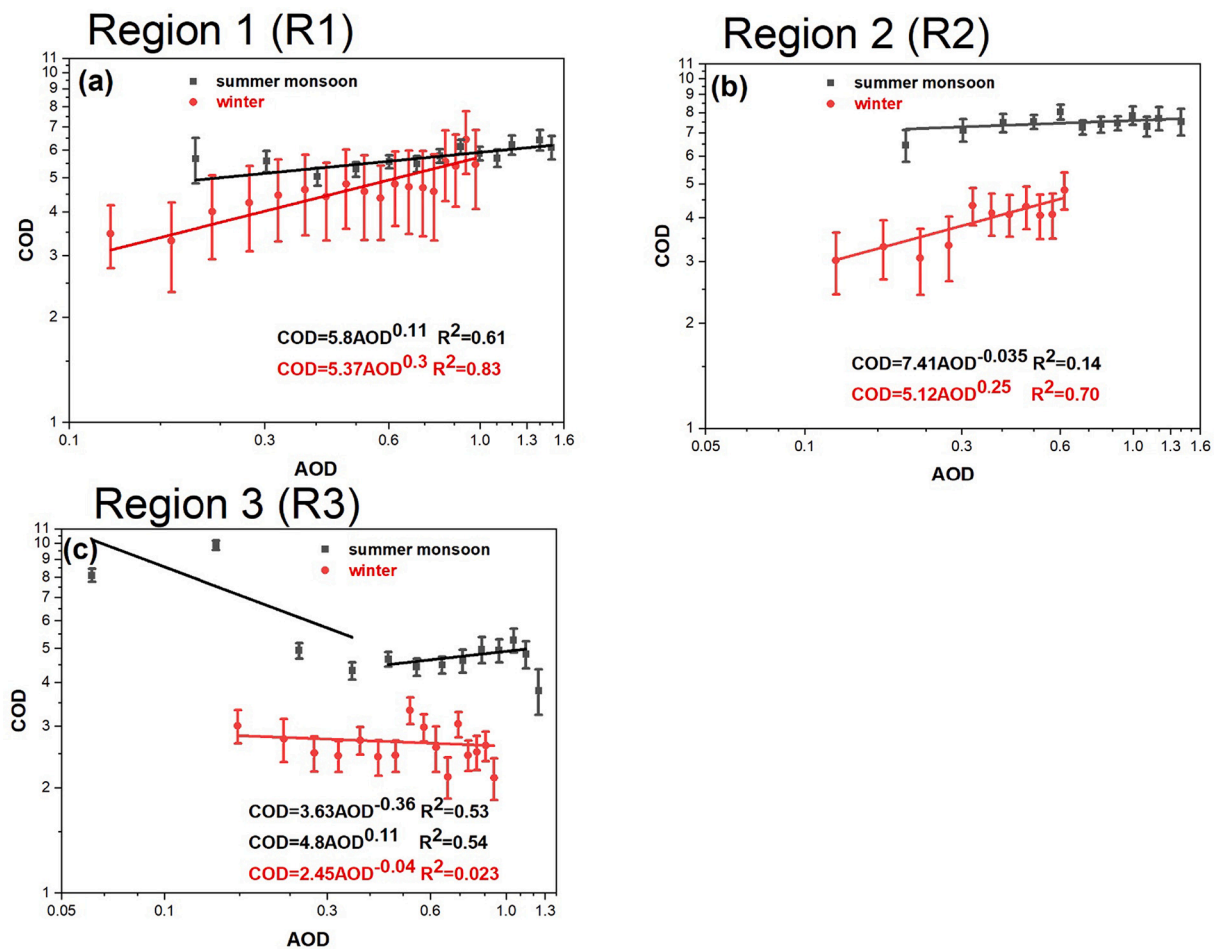


Fig. 8. Same as Fig. 6 but for the COD.

wettest condition.

3.6.2. Dynamic effect on aerosol cloud interactions

To quantify the role of dynamic motion of air parcel, the daily aerosols and clouds data are stratified into two subgroups according to the ascending air parcel ($PVV < 0$) and descending air parcel ($PVV > 0$) at 700 hPa. Both subsets are plotted on a log-log scale (see Fig. 11). It is noted that the average value of CDR is greater in descending air parcels than those in ascending air parcels, although the differences are not as significant as those of RH (see Table 1). It is also observed that the average values of CDR for $PVV < 0$ and $PVV > 0$ are almost equal (13.51 μm and 13.50 μm) over R2 (see Table 1), which indicates less influence of PVV on CDR over this region compared to other regions. This phenomenon may be attributed to the large difference in sampling sizes for the persistent upward motion ($PVV < 0$) accounting for only 26% compared to the downward motion of air parcel ($PVV > 0$) accounting for 74% of the data in R2 (see Table 1). Also, there is strong influence of PVV on the magnitude of AOD-CDR correlation over R1 (slope changes from 0.07 to 0.13) than those over R3. As shown in Table 1 the dynamic motion of air parcel over R1 is stronger (average of $PVV < 0$ are -0.17 Pa/s and $PVV > 0$ are 0.14 Pa/s) compared to R3 (average of $PVV < 0$ are -0.09 Pa/s and $PVV > 0$ are 0.09 Pa/s). Therefore, the stronger influence of PVV on AOD-CDR correlation over R1 than those of R2 and R3 may possibly associate with the systematic differences in the indicated dynamic condition of air parcel. Overall, PVV has some influence on the magnitude of AOD-CDR correlations but, cannot change the sign of AOD-CDR correlations.

3.7. Estimating first indirect effect (FIE)

In order to estimate FIE, the AOD and CDR data are sorted into various CLWP bins and then Eq. (1) (see Section 2.3) are used to compute FIE in each CLWP bin. Here the MODIS retrieved CDR and AOD data are sorted into 12, 11 and 9 CLWP bins ranging from 0 to 240, 0 to 220 with an interval of 20 g/m^2 and 0 to 90 with an interval of 10 g/m^2 over R1, R2 and R3, respectively. In order to reduce the statistical uncertainty, the CLWP bins greater than 240, 220 and 90 g/m^2 are excluded because the number of samples are appreciably less. The positive value of FIE indicate the reduction of CDR with AOD (Twomey effect) while the negative FIE indicates the growth of CDR with AOD (Anti-Twomey Effect). Most of the negative values of FIE over R1 and R2 indicate the dominance of Anti-Twomey Effect over these regions (see Fig. 12). In contrast, the positive values of FIE are found over R3 in all CLWP bins indicating the existence of Twomey effect over this region. As AOD-CDR correlation is also highly sensitive to CLWP (Jia et al., 2019). Therefore, FIE analysis reduce the role CLWP on AOD-CDR correlation.

4. Conclusion

The aerosols pollution in Pakistan has produced drastic climatic variations through direct and indirect aerosol effects. In this study, we compiled 19 years and daily aerosols and clouds data from MODIS coupled with meteorological data from ECMWF ERA-5 reanalysis data to analyze aerosol warm cloud interaction in three typical monsoon regions in Pakistan. Statistical analysis is used to figure out the aerosol indirect effect. Following are the main findings of this study.

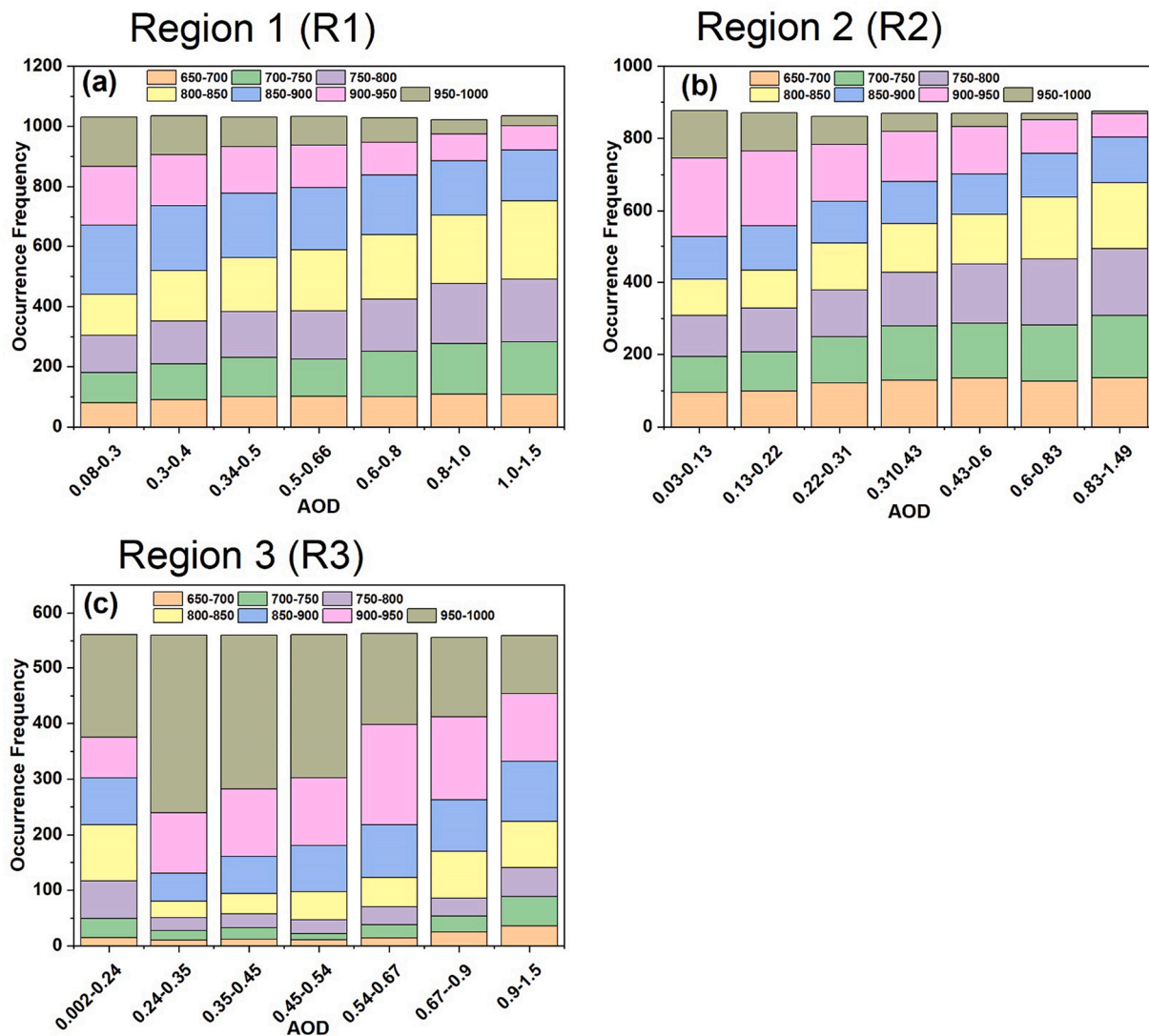


Fig. 9. Distribution frequency of CTP in various subset of AOD ranges (a) R1 (b) R2 and (c) R3.

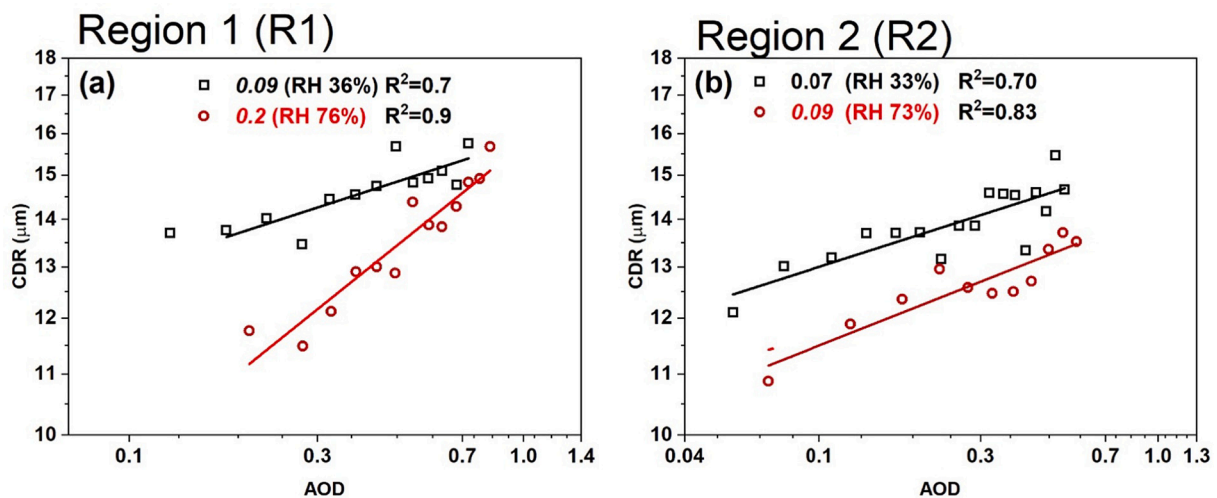


Fig. 10. AOD-CDR correlations at highest and lowest tercile of % RH over (a) R1 and (b) R2. The numbers in italic represent the slope of regression line.

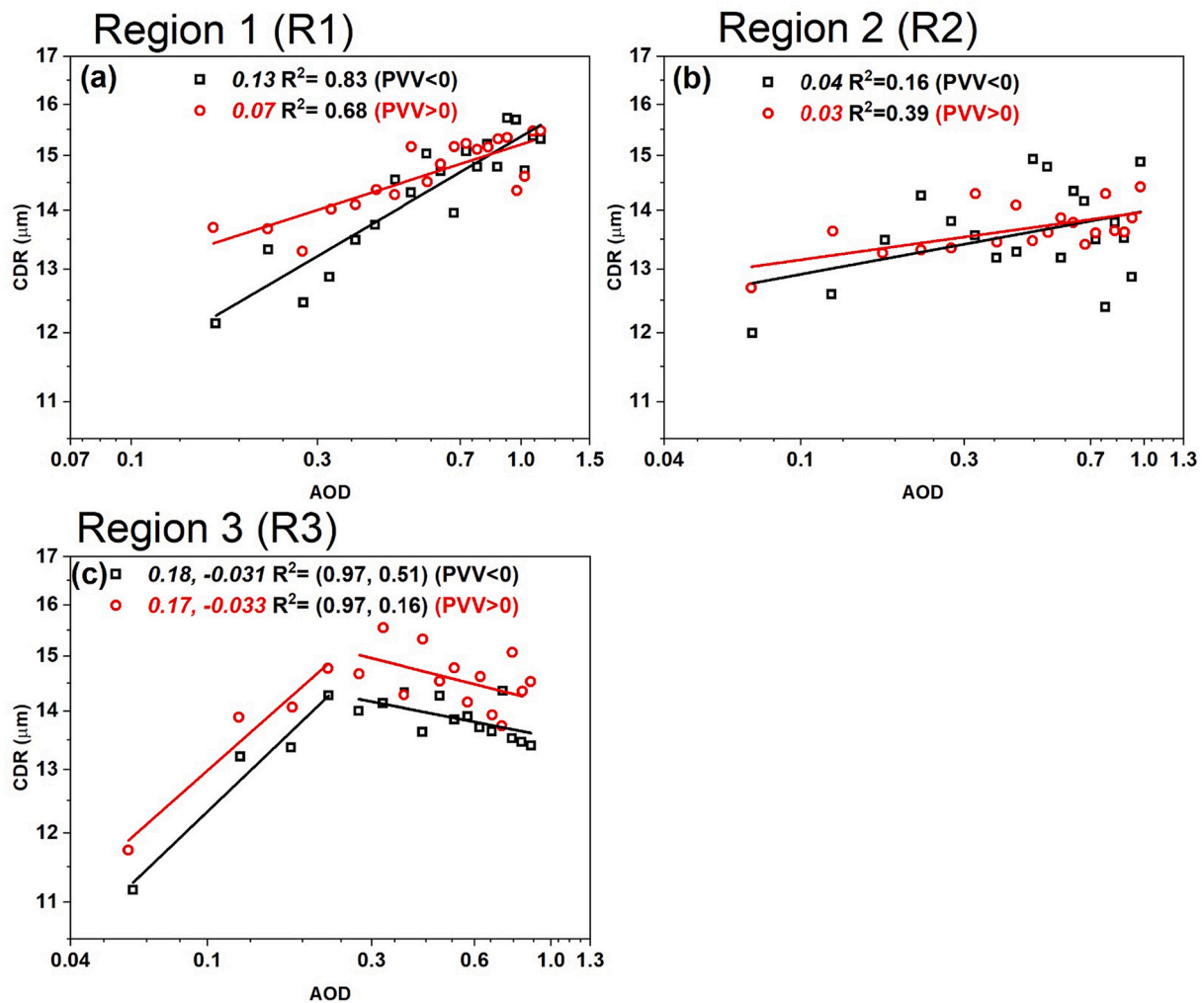


Fig. 11. Same as Fig. 10 but for the cases stratified by PVV.

Table 1
Other necessary information related to PVV influence on AOD-CDR correlations.

Region	Sampling size with (PVV < 0)	Sampling size with (PVV > 0)	Average of PVV < 0	Average of PVV > 0	Average CDR (PVV < 0)	Average CDR (PVV > 0)
R1	46%	54%	-0.17 Pa/s	0.13 Pa/s	14.30 μm	15.60 μm
R2	26%	74%	-0.14 Pa/s	0.17 Pa/s	13.51 μm	13.50 μm
R3	49%	51%	-0.093 Pa/s	0.097 Pa/s	13.56 μm	14.50 μm

- Strong seasonal variation in AOD, CDR, CLWP and COD are observed from spatio-temporal analysis over R1, R2 and R3.
- AOD-CDR, AOD-CLWP, AOD-COD correlations are found positive with the regression slope 0.09, 0.32, 0.20 over R1 and 0.04, 0.20, 0.16 over R2, respectively. Over R3, correlations have two-branches: with the regression slope 0.13, -0.82, -0.9 when AOD is less than ~0.325 and -0.13, 0.14, 0.30 at a higher AOD limit, respectively.
- Over R1 and R2, the correlations are found stronger in winter than those during the summer monsoon.
- Over R3, the correlations exhibit two branches in the summer monsoon seasons with the transitional AOD of 0.325. When AOD < 0.325, the correlations of AOD to CDR, CLWP, and COD are 0.07, -0.32, and -0.36, respectively. When AOD > 0.325, the corresponding correlations are -0.13, -0.09 and 0.11, respectively. The winter correlations are 0.06, -0.09 and 0.04 for CDR, CLWP and COD, respectively.
- An effort is also made to isolate aerosols effects from other factors such as RH and PVV. The sign of correlations is found unchanged,

with only the magnitude of correlations varies with meteorological conditions.

- The AOD-CDR correlations are found stronger at a high %RH with linear regression slope 0.2 and 0.09 over R1 and R2 compared to low %RH with slope 0.09 and 0.07.
- The AOD-CDR correlations are stronger with slope 0.13 and 0.04 when PVV < 0 than 0.07 and 0.03 when PVV > 0 over R1 and R2, respectively.

Overall, the plain terrain with elevation between (1–300 m) in R1 and R3, and hilly terrain with elevation between (300–600 m) in R2, coupled with differences in the aerosols feature layers, size, sources and concentrations (Zhang et al., 2020), makes the ACI study in the selected regions very promising. A large number of coarse mode particles with high number of aerosols feature layers over R1 than R2 (Zhang et al., 2020) make the correlations stronger over the former region as observed in this study. Also, the occurrence of both continental and marine aerosols in R3 making the correlations two folded as observed in this

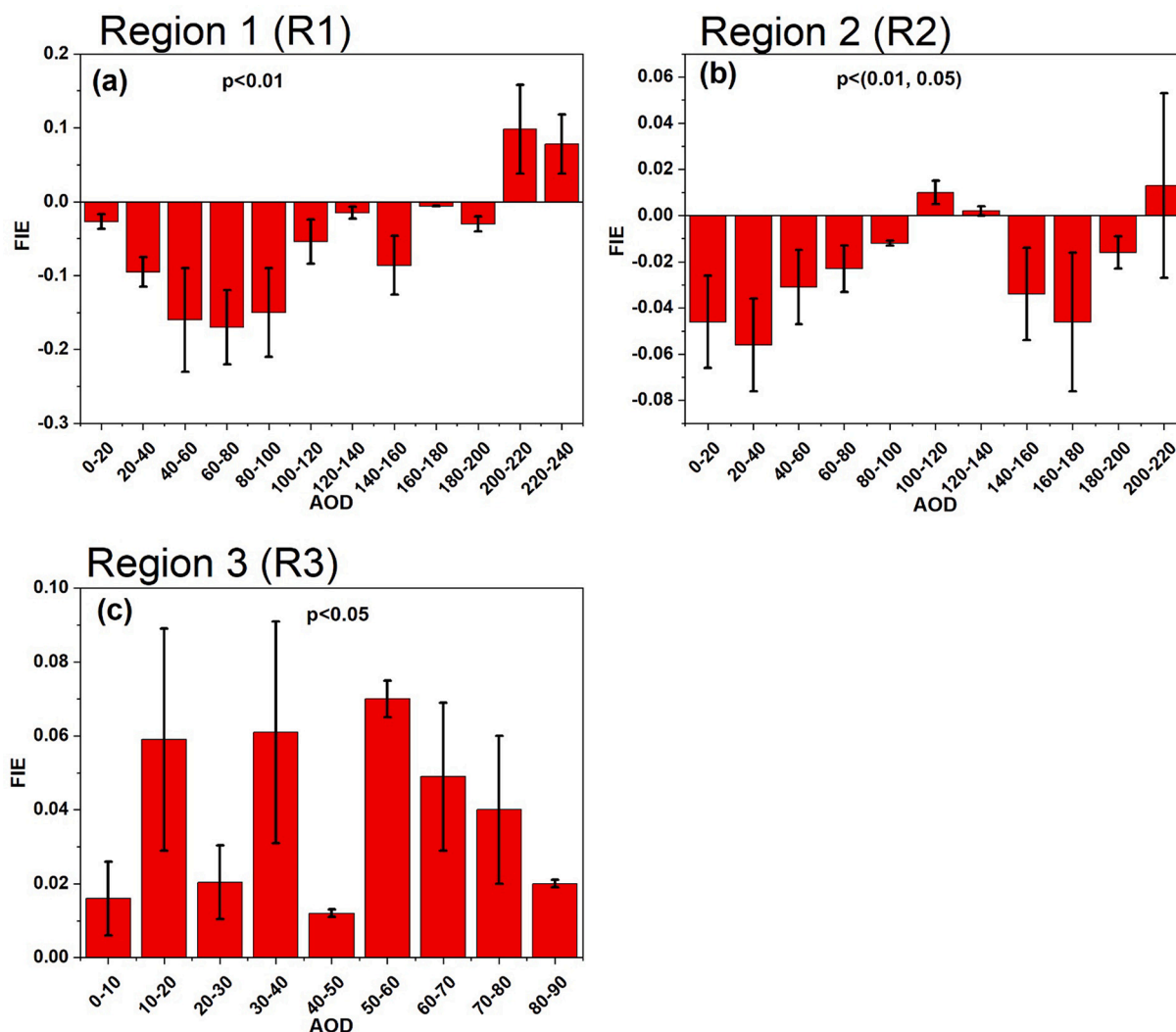


Fig. 12. (a–c) Estimate of Aerosol First Indirect Effect. Error bars represent the standard deviation.

study. The results of the study would definitely, as we believe, open a new avenue on satellite based aerosols clouds studies. The variability in ACI induced by topographical and demographical changes as distinctly brought out by our study would promote and strengthen such satellite based ACI studies by the scientific community across the globe.

Declaration of Competing Interest

The authors declare that they have no known competing financial interests or personal relationships that could have appeared to influence the work reported in this paper.

Acknowledgements

The author would like to acknowledge the substantial contribution of NASA for the provision of MODIS data. The authors also acknowledge the provision of meteorology data from ECMWF ERA-5 reanalysis data. This research was supported by Higher Education Commission (HEC) of Pakistan under the HEC NRPJ project no. 20-3582. Y. Liu is supported by the U.S. Department of Energy's Office of Energy's the Office of Science Biological and Environmental Research program as part of the Atmospheric Systems Research (ASR) program. Brookhaven National Laboratory is operated by Battelle for the U.S. Department of Energy under contract DE-SC00112704.

References

- Alam, K., Iqbal, M.J., Blaschke, T., Qureshi, S., Khan, G., 2010. Monitoring spatio-temporal variations in aerosols and aerosol–cloud interactions over Pakistan using MODIS data. *Adv. Space Res.* 46 (9), 1162–1176.
- Alam, K., Qureshi, S., Blaschke, T., 2011. Monitoring spatio-temporal aerosol patterns over Pakistan based on MODIS, TOMS and MISR satellite data and a HYSPLIT model. *Atmos. Environ.* 45 (27), 4641–4651.
- Alam, K., Khan, R., Blaschke, T., Mukhtiar, A., 2014. Variability of aerosol optical depth and their impact on cloud properties in Pakistan. *J. Atmos. Sol. Terr. Phys.* 107, 104–112.
- Albrecht, B.A., 1989. Aerosols, cloud microphysics, and fractional cloudiness. *Science* 245 (4923), 1227–1230.
- Ali, S., Khalid, B., Kiani, R.S., Babar, R., Nasir, S., Rehman, N., Goheer, M.A., 2020. Spatio-temporal variability of summer monsoon onset over Pakistan. *Asia-Pac. J. Atmos. Sci.* 56 (1), 147–172.
- Benas, N., Meirink, J.F., Karlsson, K.G., Stengel, M., Stammes, P., 2020. Satellite observations of aerosols and clouds over southern China from 2006 to 2015: analysis of changes and possible interaction mechanisms. *Atmos. Chem. Phys.* 20 (1), 457–474.
- Bilal, M., Mhawish, A., Nichol, J.E., Qiu, Z., Nazeer, M., Ali, M.A., Ke, S., 2021. Air pollution scenario over Pakistan: Characterization and ranking of extremely polluted cities using long-term concentrations of aerosols and trace gases. *Remote Sens. Environ.* 264, 112617.
- Bréon, F.M., Tanré, D., Generoso, S., 2002. Aerosol effect on cloud droplet size monitored from satellite. *Science* 295 (5556), 834–838.
- Chang, D.Y., Lelieveld, J., Tost, H., Steil, B., Pozzer, A., Yoon, J., 2017. Aerosol physicochemical effects on CCN activation simulated with the chemistry-climate model EMAC. *Atmos. Environ.* 162, 127–140.
- Chen, J., Liu, Y., Zhang, M., Peng, Y., 2016. New understanding and quantification of the regime dependence of aerosol–cloud interaction for studying aerosol indirect effects. *Geophys. Res. Lett.* 43 (4), 1780–1787.

- Chen, J., Liu, Y., Zhang, M., Peng, Y., 2018. Height dependency of aerosol-cloud interaction regimes. *J. Geophys. Res. Atmos.* 123 (1), 491–506.
- Costantino, L., Bréon, F.M., 2010. Analysis of aerosol-cloud interaction from multi-sensor satellite observations. *Geophys. Res. Lett.* 37 (11).
- Costantino, L., Bréon, F.M., 2013. Aerosol indirect effect on warm clouds over South-East Atlantic, from co-located MODIS and CALIPSO observations. *Atmos. Chem. Phys.* 13 (1), 69–88.
- Feingold, G., Remer, L.A., Ramaprasad, J., Kaufman, Y.J., 2001. Analysis of smoke impact on clouds in Brazilian biomass burning regions: an extension of Twomey's approach. *J. Geophys. Res.* 106 (D19), 22907–22922.
- Gupta, P., Khan, M.N., da Silva, A., Patadia, F., 2013. MODIS aerosol optical depth observations over urban areas in Pakistan: quantity and quality of the data for air quality monitoring. *Atmos. Pollut. Res.* 4 (1), 43–52.
- Han, Q., Rossow, W.B., Zeng, J., Welch, R., 2002. Three different behaviors of liquid water path of water clouds in aerosol–cloud interactions. *J. Atmos. Sci.* 59 (3), 726–735.
- Jeong, M.J., Li, Z., Andrews, E., Tsay, S.C., 2007. Effect of aerosol humidification on the column aerosol optical thickness over the Atmospheric Radiation Measurement Southern Great Plains site. *J. Geophys. Res. Atmos.* 112 (D10).
- Jia, H., Ma, X., Quaas, J., Yin, Y., Qiu, T., 2019. Is positive correlation between cloud droplet effective radius and aerosol optical depth over land due to retrieval artifacts or real physical processes? *Atmos. Chem. Phys.* 19 (13), 8879–8896.
- Jones, T.A., Christopher, S.A., 2008. Seasonal variation in satellite-derived effects of aerosols on clouds in the Arabian Sea. *J. Geophys. Res. Atmos.* 113 (D9).
- Jones, T.A., Christopher, S.A., Quaas, J., 2009. A six year satellite-based assessment of the regional variations in aerosol indirect effects. *Atmos. Chem. Phys.* 9 (12), 4091–4114.
- Kant, S., Panda, J., Gautam, R., 2019. A seasonal analysis of aerosol-cloud-radiation interaction over Indian region during 2000–2017. *Atmos. Environ.* 201, 212–222.
- Kim, M.K., Lau, W.K., Kim, K.M., Sang, J., Kim, Y.H., Lee, W.S., 2016. Amplification of ENSO effects on Indian summer monsoon by absorbing aerosols. *Clim. Dyn.* 46 (7–8), 2657–2671.
- Koren, I., Kaufman, Y.J., Remer, L.A., Martins, J.V., 2004. Measurement of the effect of Amazon smoke on inhibition of cloud formation. *Science* 303 (5662), 1342–1345.
- Koren, I., Kaufman, Y.J., Rosenfeld, D., Remer, L.A., Rudich, Y., 2005. Aerosol invigoration and restructuring of Atlantic convective clouds. *Geophys. Res. Lett.* 32 (14).
- Levy, R.C., Mattoo, S., Munchak, L.A., Remer, L.A., Sayer, A.M., Patadia, F., Hsu, N.C., 2013. The Collection 6 MODIS aerosol products over land and ocean. *Atmos. Meas. Tech.* 6 (11), 2989–3034.
- Liu, T., Liu, Q., Chen, Y., Wang, W., Zhang, H., Li, D., Sheng, J., 2020. Effect of aerosols on the macro- and micro-physical properties of warm clouds in the Beijing-Tianjin-Hebei region. *Sci. Total Environ.* 720, 137618.
- Liu, Q., Duan, S., He, Q., Chen, Y., Zhang, H., Cheng, N., Li, J., 2021. The variability of warm cloud droplet radius induced by aerosols and water vapor in Shanghai from MODIS observations. *Atmos. Res.* 253, 105470.
- Lohmann, U., 2002. Possible aerosol effects on ice clouds via contact nucleation. *J. Atmos. Sci.* 59 (3), 647–656.
- Lohmann, U., Lesins, G., 2003. Comparing continental and oceanic cloud susceptibilities to aerosols. *Geophys. Res. Lett.* 30 (15).
- Mahowald, N., 2011. Aerosol indirect effect on biogeochemical cycles and climate. *Science* 334 (6057), 794–796.
- Manoj, M.G., Devara, P.C.S., Joseph, S., Sahai, A.K., 2012. Aerosol indirect effect during the aberrant Indian Summer Monsoon breaks of 2009. *Atmos. Environ.* 60, 153–163.
- Masmoudi, M., Chaabane, M., Tanré, D., Gouloup, P., Blarel, L., Elleuch, F., 2003. Spatial and temporal variability of aerosol: size distribution and optical properties. *Atmos. Res.* 66 (1–2), 1–19.
- Miltenberger, A.K., Field, P.R., Hill, A.A., Rosenberg, P., Shipway, B.J., Wilkinson, J.M., Blyth, A.M., 2018. Aerosol–cloud interactions in mixed-phase convective clouds—part 1: Aerosol perturbations. *Atmos. Chem. Phys.* 18 (5), 3119–3145.
- Minnis, P., Heck, P.W., Young, D.F., Fairall, C.W., Snider, J.B., 1992. Stratocumulus cloud properties derived from simultaneous satellite and island-based instrumentation during FIRE. *J. Appl. Meteorol. Climatol.* 31 (4), 317–339.
- Myhre, G., Stordal, F., Johnsrud, M., Kaufman, Y.J., Rosenfeld, D., Storelvmo, T., Isaksen, I.S., 2007. Aerosol-cloud interaction inferred from MODIS satellite data and global aerosol models. *Atmos. Chem. Phys.* 7 (12), 3081–3101.
- Nakajima, T., Higurashi, A., Kawamoto, K., Penner, J.E., 2001. A possible correlation between satellite-derived cloud and aerosol microphysical parameters. *Geophys. Res. Lett.* 28 (7), 1171–1174.
- Ou, S.C., Liou, K.N., Hsu, N.C., Tsay, S.C., 2012. Satellite remote sensing of dust aerosol indirect effects on cloud formation over Eastern Asia. *Int. J. Remote Sens.* 33 (22), 7257–7272.
- Pan, Z., Mao, F., Wang, W., Logan, T., Hong, J., 2018. Examining intrinsic aerosol-cloud interactions in South Asia through multiple satellite observations. *J. Geophys. Res. Atmos.* 123 (19), 11–210.
- Papadimas, C.D., Hatzianastassiou, N., Mihalopoulos, N., Kanakidou, M., Katsoulis, B.D., Vardavas, I., 2009. Assessment of the MODIS Collections C005 and C004 aerosol optical depth products over the Mediterranean basin. *Atmos. Chem. Phys.* 9 (9), 2987–2999.
- Platnick, S., Meyer, K.G., King, M.D., Wind, G., Amarasinghe, N., Marchant, B., Riedi, J., 2016. The MODIS cloud optical and microphysical products: Collection 6 updates and examples from Terra and Aqua. *IEEE Trans. Geosci. Remote Sens.* 55 (1), 502–525.
- Qiu, Y., Zhao, C., Guo, J., Li, J., 2017. 8-year ground-based observational analysis about the seasonal variation of the aerosol-cloud droplet effective radius relationship at SGP site. *Atmos. Environ.* 164, 139–146.
- Quan, J., Gao, Y., Zhang, Q., Tie, X., Cao, J., Han, S., Zhao, D., 2013. Evolution of planetary boundary layer under different weather conditions, and its impact on aerosol concentrations. *Particology* 11 (1), 34–40.
- Rao, S., Dey, S., 2020. Consistent signal of aerosol indirect and semi-direct effect on water clouds in the oceanic regions adjacent to the Indian subcontinent. *Atmos. Res.* 232, 104677.
- Rasmusson, E.M., Carpenter, T.H., 1983. The relationship between eastern equatorial Pacific Sea surface temperatures and rainfall over India and Sri Lanka. *Mon. Weather Rev.* 111 (3), 517–528.
- Remer, L.A., Kaufman, Y.J., Tanré, D., Mattoo, S., Chu, D.A., Martins, J.V., Holben, B.N., 2005. The MODIS aerosol algorithm, products, and validation. *J. Atmos. Sci.* 62 (4), 947–973.
- Rosenfeld, D., 2000. Suppression of rain and snow by urban and industrial air pollution. *Science* 287 (5459), 1793–1796.
- Safdar, F., Khokhar, M.F., Arshad, M., Adil, I.H., 2019. Climate change indicators and spatiotemporal shift in monsoon patterns in Pakistan. *Adv. Meteorol.* 2019.
- Saponaro, G., Kolmonen, P., Sogacheva, L., Rodriguez, E., Virtanen, T., Leeuw, G.D., 2017. Estimates of the aerosol indirect effect over the Baltic Sea region derived from 12 years of MODIS observations. *Atmos. Chem. Phys.* 17 (4), 3133–3143.
- Sarangi, C., Tripathi, S.N., Kanawade, V.P., Koren, I., Pai, D.S., 2017. Investigation of the aerosol–cloud–rainfall association over the Indian summer monsoon region. *Atmos. Chem. Phys.* 17 (8), 5185–5204.
- Sharif, F., Alam, K., Afsar, S., 2015. Spatio-temporal distribution of aerosol and cloud properties over Sindh using MODIS satellite data and a HYSPLIT model. *Aerosol Air Qual. Res.* 15 (2), 657–672.
- Small, J.D., Jiang, J.H., Su, H., Zhai, C., 2011. Relationship between aerosol and cloud fraction over Australia. *Geophys. Res. Lett.* 38 (23).
- Sporre, M.K., Swietlicki, E., Glantz, P., Kulmala, M., 2014. A long-term satellite study of aerosol effects on convective clouds in Nordic background air. *Atmos. Chem. Phys.* 14 (4), 2203–2217.
- Storelvmo, T., Kristjánsson, J.E., Myhre, G., Johnsrud, M., Stordal, F., 2006. Combined observational and modeling based study of the aerosol indirect effect. *Atmos. Chem. Phys.* 6 (11), 3583–3601.
- Tariq, S., Ali, M., 2015. Spatio-temporal distribution of absorbing aerosols over Pakistan retrieved from OMI onboard Aura satellite. *Atmos. Pollut. Res.* 6 (2), 254–266.
- Tripathi, S.N., Pattnaik, A., Dey, S., 2007. Aerosol indirect effect over Indo-Gangetic plain. *Atmos. Environ.* 41 (33), 7037–7047.
- Twohy, C.H., Durkee, P.A., Huebert, B.J., Charlson, R.J., 1995. Effects of aerosol particles on the microphysics of coastal stratiform clouds. *J. Clim.* 8 (4), 773–783.
- Twomey, S.J., 1974. Pollution and the planetary albedo. *Atmos. Environ.* (1967) 8 (12), 1251–1256.
- Wang, F., Guo, J., Wu, Y., Zhang, X., Deng, M., Li, X., Zhao, J., 2014. Satellite observed aerosol-induced variability in warm cloud properties under different meteorological conditions over eastern China. *Atmos. Environ.* 84, 122–132.
- Wang, F., Guo, J., Zhang, J., Huang, J., Min, M., Chen, T., Li, X., 2015. Multi-sensor quantification of aerosol-induced variability in warm clouds over eastern China. *Atmos. Environ.* 113, 1–9.
- Xie, X., Wang, H., Liu, X., Li, J., Wang, Z., Liu, Y., 2016. Distinct effects of anthropogenic aerosols on the East Asian summer monsoon between multidecadal strong and weak monsoon stages. *J. Geophys. Res. Atmos.* 121 (12), 7026–7040.
- Xue, H., Feingold, G., Stevens, B., 2008. Aerosol effects on clouds, precipitation, and the organization of shallow cumulus convection. *J. Atmos. Sci.* 65 (2), 392–406.
- Yuan, T., Li, Z., Zhang, R., Fan, J., 2008. Increase of cloud droplet size with aerosol optical depth: an observation and modeling study. *J. Geophys. Res. Atmos.* 113 (D4).
- Zeb, B., Alam, K., Sorooshian, A., Chishtie, F., Ahmad, I., Bibi, H., 2019. Temporal characteristics of aerosol optical properties over the glacier region of northern Pakistan. *J. Atmos. Sol. Terr. Phys.* 186, 35–46.
- Zhang, M., Su, B., Bilal, M., Atique, L., Usman, M., Qiu, Z., Han, G., 2020. An investigation of vertically distributed aerosol optical properties over Pakistan using CALIPSO satellite data. *Remote Sens.* 12 (14), 2183.
- Zhao, X., Liu, Y., Yu, F., Heindinger, A.K., 2018. Using long-term satellite observations to identify sensitive regimes and active regions of aerosol indirect effects for liquid clouds over global oceans. *J. Geophys. Res. Atmos.* 123 (1), 457–472.